ERDC/EL TR-22-3

US Army Corps
of Engineers®
Engineer Research and
Development Center

ERDC
ENGINEER RESEARCH & DEVELOPMENT CENTER

Toward the Electrochemical Detection of 2,4-Dinitroanisole (DNAN) and Pentaerythritol Tetranitrate (PETN)

Matthew W. Glasscott, Johanna N. Jernberg, Erik M. Alberts, and Lee C. Moores

March 2022

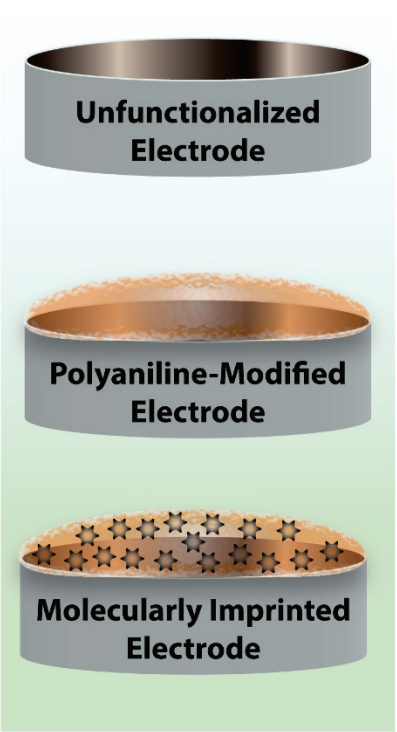

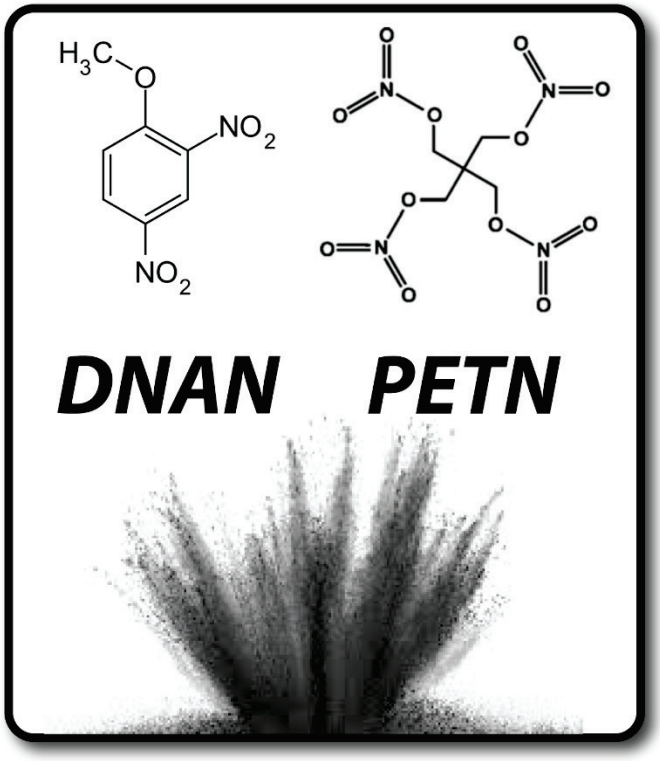

Environmental Laboratory

The U.S. Army Engineer Research and Development Center (ERDC) solves the nation's toughest engineering and environmental challenges. ERDC develops innovative solutions in civil and military engineering, geospatial sciences, water resources, and environmental sciences for the Army, the Department of Defense, civilian agencies, and our nation's public good. Find out more at www.erdc.usace.army.mil.

To search for other technical reports published by ERDC, visit the ERDC online library at https://erdclibrary.on.worldcat.org/discovery.

ERDC/EL TR-22-3
March 2022

Progress toward the Electrochemical Detection of 2,4-Dinitroanisole (DNAN) and Pentaerythritol Tetranitrate (PETN)

Matthew W. Glasscott and Lee C. Moores

US Army Engineer Research and Development Center (ERDC)
Environmental Laboratory (EL)
3909 Halls Ferry Rd
Vicksburg, MS 39180-6199

Johanna N. Jernberg

Oak Ridge Institute for Science and Education
1299 Bethel Valley Rd.
Oak Ridge, TN 37830

Erik M. Alberts

SIMETRI
7005 University Blvd.
Winter Park, FL 32792

Final report

Prepared for Headquarters, U.S. Army Corps of Engineers
Washington, DC 20314-1000

Under Project 494498, "Understanding the Environment as a Threat (UET)"
Program Element Number U452567
Task Number A1000

Abstract

Analytical methods to rapidly detect explosive compounds with high precision are paramount for applications ranging from national security to environmental remediation. This report demonstrates two proof-of-concept electroanalytical methods for the quantification of 2,4-dinitroanisol (DNAN) and pentaerythritol tetranitrate (PETN). For the first time, DNAN reduction was analyzed and compared at a bare graphitic carbon electrode, a polyaniline-modified (PANI) electrode, and a molecularly imprinted polymer (MIP) electrode utilizing PANI to explore the effect of surface-area and preconcentration affinity on the analytical response.

Since some explosive compounds such as PETN are not appreciably soluble in water (<10 μg/L), necessitating a different solvent system to permit direct detection *via* electrochemical reduction. A 1,2-dichloroethane system was explored as a possibility by generating a liquid-liquid extraction-based sensor exploiting the immiscibility of 1,2-dichloroethane and water. The reduction process was explored using a scan rate analysis to extract a diffusion coefficient of 6.67×10^{-6} cm/s, in agreement with literature values for similarly structured nitrate esters.

Once further refined, these techniques may be extended to other explosives and combined with portable electrochemical hardware to bring real-time chemical information to soldiers and citizens alike.

Contents

Abstract ii

Figures iv

Preface v

1 Introduction 1

1.1 Background 1
1.2 Objectives 2
1.3 Approach 2

2 Experimental Methods 3

2.1 Materials 3
2.2 Instrumentation 3
2.3 Electrochemical methodology and parameters 3

3 Results and Discussion 5

3.1 Characterization and optimization of screen-printed electrodes 5
3.2 Redox evaluation of model nitroaromatic compounds for matrix selection 9
3.3 Electropolymerization and characterization of polyaniline-modified sensors 11
3.4 Detection of DNAN using polyaniline-modified sensors 15
3.5 Assessment of DNAN/polyaniline molecularly imprinted polymer (MIP) sensor 19
3.6 Evaluation of PETN in liquid-liquid extraction amenable 1,2-dichloroethane 22

4 Conclusions and Future work 27

References 29

Acronyms and Abbreviations 33

Report Documentation Page

Figures

Figure 1. Generic screen-printed electrode along with cyclic voltammograms showing sensor-to-sensor variation in 1 mM Ferrocene methanol. 6

Figure 2. Effect of CSWV pulse period on the resulting capacitive background signal. 8

Figure 3. CSWV showing the effect of Ag contamination on the electrochemical signal. 9

Figure 4. Electroreduction of a single nitroaromatic group on TNT. 10

Figure 5. Effect of pH on the electroreduction of TNT. 11

Figure 6. (a) Electropolymerization of aniline to form a conductive PANI film; (b) Micrograph of unmodified working electrode; (c) Post-PANI modification micrograph. 13

Figure 7. Current magnitude as a function of incubation time demonstrating the preconcentration effect of DNAN within the PANI film. 14

Figure 8. Electrochemical cleaning procedure to extract DNAN from the PANI-thin film. 15

Figure 9. Comparison of unmodified carbon electrode and the PANI-modified electrode revealing a 4x current enhancement. 16

Figure 10. Reduction of DNAN at a PANI-modified surface after a 5-min preconcentration timeframe. 17

Figure 11. (a) Baseline corrected and subtracted SWVs from Figure 10; (b) Calibration curve obtained from the SWV data. 19

Figure 12. Overlay of electropolymerization voltammograms for the MIP and NIP. 20

Figure 13. Competing current/capacitive responses for the MIP at various concentrations of DNAN. 21

Figure 14. Peak current versus concentration of DNAN revealing capacitive/electron transfer competition. 22

Figure 15. (a) Cyclic voltammograms at various concentrations of PETN in deaerated 1,2-dichloroethane; (b) Calibration curve tracking the peak height as a function of concentration. 24

Figure 16. Scan rate analysis to determine diffusion versus surface control. 25

Figure 17. (a) Non-linear trend for peak current plotted against the scan; (b) Linear trend for peak current for PETN reduction plotted against the square-root of the scan rate. 25

Figure 18. Control experiment assessing the anodic and cathodic capacitive current signal (surface controlled) as a function of scan rate. 26

Preface

This study was conducted for the Environmental Quality and Installations Research Program under 489630, "Understanding the Environment as a Threat, Subterranean Network Interrogation Platform." The technical monitor was Dr. Christa Woodley, Engineer Research and Development Center-Environmental Laboratory (ERDC-EL).

The work was performed by the Environmental Chemistry Branch (EPC) of the Environmental Processes Division (EP), ERDC-EL. At the time of publication, Ms. Amber L. Russell was Chief, EPC; Mr. Warren Lorentz was Chief, EP; and Dr. Elizabeth A. Ferguson, ETZ was the Technical Director for Installations and Operational Environments. The ERDC-EL Deputy Directors were Dr. Brandon Lafferty and Dr. Jack Davis, and the Director was Dr. Edmund Russo.

COL Teresa A. Schlosser was Commander of ERDC, and Dr. David W. Pittman was the Director.

1 Introduction

1.1 Background

Reliable methods for the sensitive and specific detection of explosives are essential for promoting security and safety for Warfighters and civilians alike. The recent deployment of insensitive munitions involved the replacement of 2,4,6-trinitrotoluene (TNT) with 2,4-dinitroanisole (DNAN) (Stanley et al. 2015). However, its pervasive use introduces the potential for DNAN contamination of industrial wastewaters and soil near firing ranges. Studies evaluating the environmental fate of DNAN suggest resistance to biodegradation and persistence in natural systems (Perreault et al. 2012; Hawari et al. 2015; Olivares et al. 2013). Thus, the development of strategies for detecting DNAN in-field is essential to inform remediation efforts. There is also a need for detection strategies for pentaerythritol tetranitrate (PETN), which is sparingly soluble in water, but up to five times more toxic than 1,3,5-trinitro-1,3,5-triazine (RDX) for aquatic species (Zhuang et al. 2008).

Analytical methods applied for the detection of nitro-containing explosives include mass spectrometry (MS) (Ewing et al. 2013), ion mobility spectrometry (IMS) (Tam and Hill 2004), surface enhanced Raman spectroscopy (SERS) (Dasary et al. 2009), and colorimetric analysis (Forzani et al. 2009). While exhibiting excellent sensitivity and selectivity, the need for expert technicians and the relative cost-per-sample of mass spectrometry-based methods excludes their point-of-use application. IMS-based detection is commonly employed for airport security, but generally relies on vapor-phase detection and shows poor selectivity (Eiceman et al. 2004). While exhibiting excellent limits of detection, the reproducibility of SERS is highly dependent on the substrate employed (Demeritte et al. 2012). Colorimetric techniques offer simple visual results, but generally require high concentrations of analyte to trigger a response.

In contrast, electrochemical methods are characterized by low costs (Glasscott et al. 2020), high sensitivity (particularly when preconcentration methods [Fernando et al. 2021], or surface functionalization [Glasscott and Dick 2021; Glasscott et al. 2018; Glasscott et al. 2020] is employed), and specificity based on the unique electron transfer potentials exhibited by different analytes (Bard and Faulkner

2001). Compounds such as DNAN and PETN are excellent candidates for electrochemical detection due to the electron-accepting (reduction) reactivity of the respective nitro and nitrate ester-groups characteristic to each structure. Thus, exploring the fundamental electron transfer properties and the effect of electrode surface structure on the analytical response is worthy of pursuit towards low cost, deployable sensors.

1.2 Objectives

This work seeks to explore fundamental approaches for detecting DNAN and PETN using solution-phase electrochemistry. Since nitro and nitrate ester groups are subject to reduction, electrochemistry represents a viable route for specific and selective detection of both compounds. Due to differences in solubility, two separate detection media were explored; an aqueous phase reduction for DNAN amenable to environmental systems and an organic phase reduction for PETN, which may serve as the basis for liquid-liquid extraction techniques in the future. Characterization of the electrochemical signal for both compounds with various electrode modifications will inform the future development of deployable sensors.

1.3 Approach

The reduction of both nitro-moieties on the DNAN structure were evaluated by square wave voltammetry (SWV) to probe limits of detection with three electrodes: a bare graphitic carbon electrode, a polyaniline (PANI)-modified electrode, and a DNAN/PANI molecularly imprinted polymer (MIP) electrode. We hypothesize the enhanced surface area provided by the conductive polyaniline would enhance the analytical response over the bare electrode, with further enhancement when the polymer is imprinted with the molecular template. Furthermore, we hypothesize that at least one of the four nitrate ester groups on PETN would undergo a redox reaction within the solvent window of 1,2-dichloroethane to facilitate liquid-liquid extraction-type sensing experiments.

2 Experimental Methods

2.1 Materials

The reagents 2,4-dinitroanisole (DNAN), pentaerythritol tetranitrate (PETN), and 2,4,6-trinitrotoluene (TNT) were obtained as 1,000 ppm standards in MeOH from AccuStandard (New Haven, CT). Ferrocene methanol (97%), tetrabutylammonium hexafluorophosphate (98%), 10x M phosphate buffered saline, sodium acetate (99.5%), glacial acetic acid, sodium carbonate (98%), sodium bicarbonate (98%), and potassium chloride (99.9%) were purchased from MilliporeSigma (St. Louis, MO). 1,2-dichloroethane (98%) was purchased from Fisher Scientific (Hampton, NH) and high-purity water was obtained from a MilliporeSigma Milli-Q system with a resistivity ≥ 18.2 MΩ cm^{-1}.

2.2 Instrumentation

All electrochemical experiments were carried out using a Pine WaveDriver potentiostat (Durham, NC) and aftermath software was used to facilitate all experiments. A glassy carbon working electrode (3 mm diameter, CH Instruments, Austin, TX), a silver/silver ion reference electrode, and a Pt wire counter electrode were used for experiments in 1,2-dichloroethane regarding PETN detection. Carbon screen-printed electrodes (2 mm working electrode, Ag/AgCl pseudo-reference electrode, and carbon counter electrode) were obtained from BASI (West Lafayette, IN).

Scanning electron microscopy (SEM) imaging was done using a Phenom Pharos Desktop SEM from Thermo Fisher Scientific (MA, USA) operating in backscatter detection mode at 15 keV.

2.3 Electrochemical methodology and parameters

For experiments related to DNAN, the carbon screen-printed electrodes (SPE) were rinsed with Milli-Q water prior to use. All experiments used a 5 mL volume of the indicated solution in a 10 mL beaker so the SPE surface could be brought just below the solution level. Characterization experiments examined the oxidation response of 1 mM ferrocene methanol in 1x PBS from 0 – 400 mV vs Ag/AgCl at 100 mV/s. For polymerization experiments, cyclic voltammograms were carried out with 110 mM aniline in 0.5 M H_2SO_4 from -100 to 1000 mV vs Ag/AgCl at 100 mV/s for 10 cycles. For the formation of a DNAN molecularly imprinted polymer, 0.5

mM DNAN was introduced so the solubility limit of DNAN was not exceeded, and an equivalent polymerization procedure was conducted. For the detection of DNAN, SWV was employed from -0.3 to -1.3 V vs Ag/AgCl with the following parameters: equilibrium time: 10 s @ 1300 mV, potential increment 3 mV, pulse potential 30 mV, pulse period 50 ms, sampling period 1 ms. The solution was static during testing but stirred during incubation and extraction periods using a rotating Teflon stir bar and stir plate.

For PETN-related experiments, the glassy carbon electrode was polished with 1, 0.3, and 0.05 μm alumina paste and cleaned with distilled water prior to use. A solution of 0.1 M tetrabutylammonium hexafluorophosphate was introduced as a supporting electrolyte and was purged for 5 min prior to experimentation using argon gas. Cyclic voltammograms were used to detect PETN from 0 to -1.5 V vs Ag/Ag^{+} at 0.1 V/s. Scan rate experiments employed the following scan rates: 10, 25, 50, 100, 250, and 500 mV/s.

3 Results and Discussion

3.1 Characterization and optimization of screen-printed electrodes

Although they are relatively expensive, inert surfaces such as polycrystalline platinum, gold, and glassy carbon have been used as standard electrode materials due to their processability *via* polishing to restore the surface to a pristine condition (Elgrishi et al. 2018). Thus, SPEs, which incorporate a thin-film, non-polishable sensing electrode surface, are most amenable to deployable sensing due to their low cost. Figure 1 shows a close-up image of a generic SPE with relevant electrodes labeled. The sensing electrode (working electrode) is generally a disk shape to permit mathematical modeling of the diffusion profile about the electrode surface (Ngamchuea et al. 2014). The counter electrode completes the circuit and has a higher area than the working electrode. This is to reduce the compensating voltage necessary to set the potential of the working electrode so various reactions may be driven. To improve the accuracy of the potential set at the working electrode and provide conversion from electrical voltage values to chemical voltage values, a reference electrode composed of an Ag/AgCl interface covered in a polymeric paste to prevent leaching is also incorporated. Generally, the printing process proceeds using vapor deposition or spray printing of a micrometer-thick conductive layer onto the substrate, which is polyethylene terephthalate in the image. For experiments detailed below, electrodes similar to that shown in Figure 1 were used but printed on ceramic substrates with a carbon working and counter electrode, and an Ag/AgCl paste reference electrode.

Figure 1. Generic screen-printed electrode along with cyclic voltammograms showing sensor-to-sensor variation in 1 mM Ferrocene methanol.

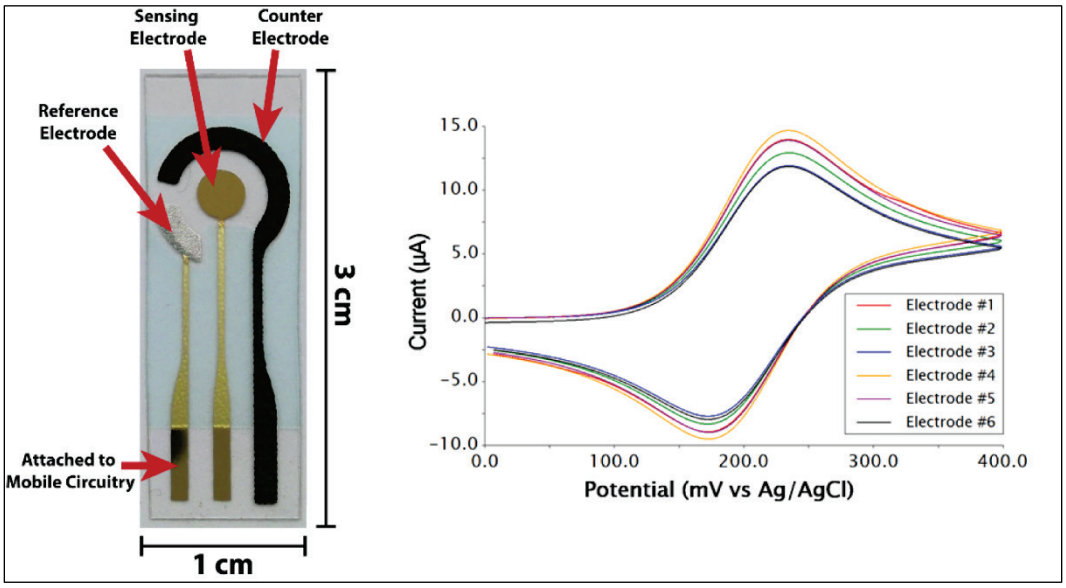

Unfortunately, the nature of the graphitic ink introduces significant heterogeneity in surface structure on the working electrode (Wang et al. 1998). While traditional polished electrodes may be modeled as two-dimensional geometric disks, the three-dimensional structure of the SPE surface may lead to variations in the electrochemically active surface area and, thus, the analytical electrochemical signal. For instance, Figure 1 shows a series of cyclic voltammograms performed over six SPEs, which all show varying current responses for the oxidation of ferrocene methanol. The scan begins at 0 V, sweeps to 0.4 V producing a peak related to the oxidation of ferrocene methanol, then sweeps back to 0 V producing a peak related to the reduction of the ferrocenium methanol cation. Since ferrocene methanol is an outer-sphere electron transfer molecule, it may be used to report the electrochemically active surface area of a given electrode (assuming a semi-infinite linear diffusion profile [Ngamchuea et al. 2014]), as the peak current is directly proportional to the electrode area according to the Randles-Sevcik equation:

$$i_p = 268{,}600 n^{3/2} C^* A D^{1/2} v^{1/2}$$

Where n is the number of electrons, C^* is the bulk concentration of the analyte, D is the diffusion coefficient of the analyte, A is the electrode area, and v is the scan rate. Using the radius of the screen-printed electrodes employed (2 mm), the diffusion coefficient of ferrocene methanol (7.0 x 10^{-6} cm/s) (Cannes et al. 2003), a concentration of 1 mM, and a scan rate

(0.1 V/s), one would predict a peak current of *ca.* 7.5 μA. However, the peak current obtained exceeds this value because of the non-geometric nature of the graphitic SPE surface. This heterogeneity is observed in the relative spread of peak currents, meaning sensors based on redox chemistry will reflect an uncertainty interval proportional to the difference in area electrode-to-electrode.

While cyclic voltammetry is a popular means of evaluating electron transfer (Faradaic) processes, a significant capacitive current related to ion rearrangement (non-Faradaic) processes at the electrode surface can masks important peaks and features which may be used for chemical sensing. This phenomenon is particularly significant at high-surface area electrodes (i.e., porous, rough) (de Levie 1963), including the polymer-modified electrodes used in this work. To reduce the capacitive current, square wave voltammetry (SWV, also cyclic square wave voltammetry, CSWV, if two sweeps are applied) uses alternating current pulses to background subtract the capacitive signal from the analytical signal. This is possible due to the rapid decay of ion rearrangement processes at the electrode surface compared to the relatively slow decay of diffusion-controlled electron transfer processes. However, the pulse parameters must be optimized to obtain voltammograms free of significant capacitance. For example, Figure 2 shows two CSWVs, one obtained with a 50 ms pulse period and the other with a 20 ms pulse period. Importantly, a sampling period of 1 ms was maintained at the conclusion of the pulse period. The 50 ms pulse period provides a voltammogram with a lower background current because the decay of the capacitive signal happens over a longer timeframe. Conversely, the 20 ms pulse period produces a larger background due to the higher fraction of capacitive signal captured in the 1 ms sampling period.* Based on these results, a 50 ms pulse period was utilized throughout these experiments for the evaluation of polymer-modified and molecularly imprinted electrodes.

* For further information on SWV parameters and optimization, see Bard and Faulkner 2001.

Figure 2. Effect of CSWV pulse period on the resulting capacitive background signal.

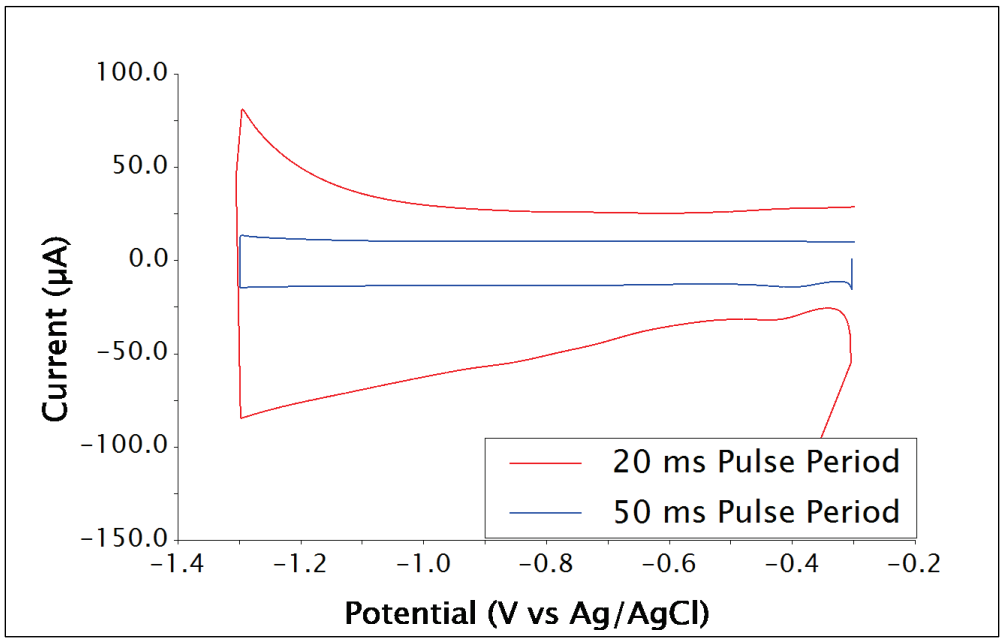

As previously mentioned, the reference electrode surface is composed of an Ag/AgCl interface covered with a polymeric paste to prevent silver leaching. This interface provides a stable reference potential allowing electrochemical processes to be calibrated thermodynamically; however, if exposed to the solution for an extended period of time (hours), silver ions may escape the polymer diffusion barrier and contaminate the matrix, or even deposit spontaneously on the working electrode surface *via* photodeposition. The effect of silver ion in solution can easily be observed using voltammetry, as silver ion will be reduced on the surface and re-oxidized at mild potentials. Figure 3 shows a voltammogram of an SPE left in 1x phosphate buffered saline (PBS) overnight. Scanning toward negative voltages, no peak is observed until *ca.* -0.5 V versus Ag/AgCl, where oxygen reduction to hydrogen peroxide begins to manifest. After this wave, a small sharp deposition peak is observed before the scan reverses back toward positive voltages. At *ca.* 0.25 V vs Ag/AgCl, a large symmetric surface peak is observed, which is consistent with Ag^0 oxidation to Ag^+ *via* a 1 electron process. Thus, it is important to minimize SPE contact with a solution for prolonged periods of time to protect the surface integrity of the working electrode. The decomposition of the reference electrode will result in potential drifting, which could hamper analytical characterization of peaks based on their thermodynamic position relative to Ag/AgCl.

Figure 3. CSWV showing the effect of Ag contamination on the electrochemical signal.

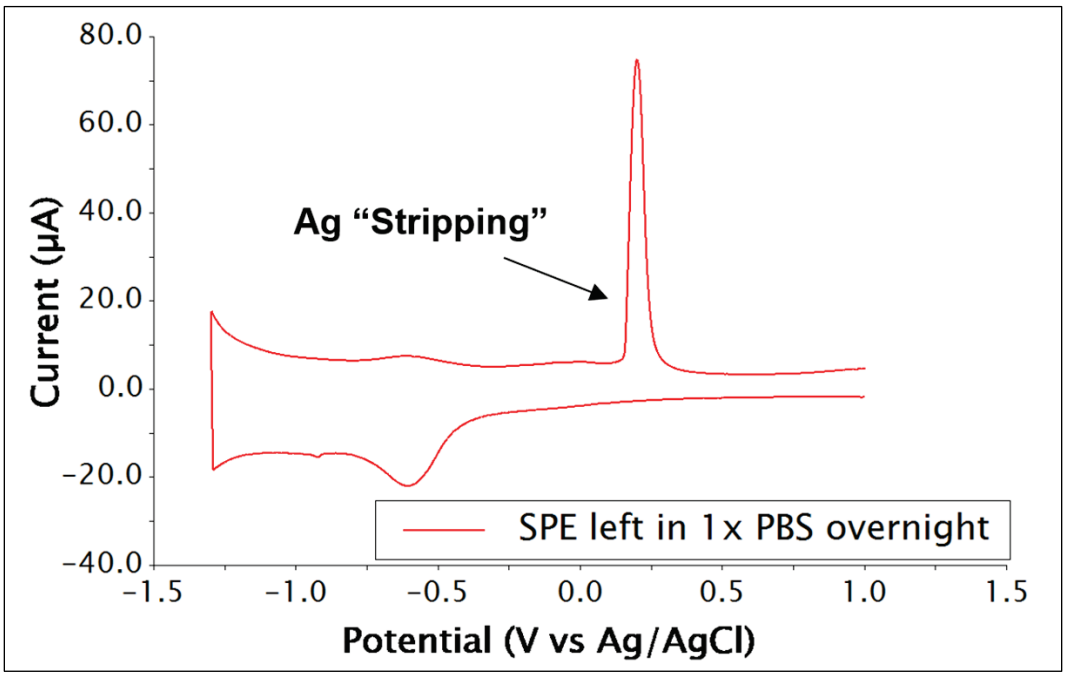

3.2 Redox evaluation of model nitroaromatic compounds for matrix selection

To optimize the SPE sensors for the detection of nitroaromatic compounds, the electrochemical response in various buffers was evaluated using a model compound, 2,4,6-trinitrotoluene (TNT). Nitroaromatic reduction reactions are commonly studied in the electrochemical literature and proceed through a proton-coupled reaction to produce primary amines (Galik et al. 2011). Though more complicated mechanisms have been reported, generally the reduction of nitroaromatic groups follows the reaction pathway below:

$$Ar-NO_2 \xrightarrow[+2e^- +2H^+ -H_2O]{} Ar-NO \xrightarrow[+2e^- +2H^+]{} Ar-NH(OH) \xrightarrow[+2e^- +2H^+ -H_2O]{} Ar-NH_2$$

Notably, each step in this reaction progression is reversible, meaning the reduced amine may be oxidized back to a nitro-group at sufficient potentials (Galik et al. 2011). This reaction was examined in 0.1 M PBS to evaluate the electrochemical response (Figure 4). The background voltammogram shows characteristics of oxygen reduction manifesting as an increase in current at more negative potentials, but no discrete peaks. When 10 mg/L TNT was added, a significant reduction peak at *ca.* -0.45 V vs Ag/AgCl appears over the background, corresponding to the reduction of a single nitro-group to an amine (Galik et al. 2011). If the potential was

swept further negative, two other reduction peaks related to the two other nitro groups on TNT appeared, though these peaks were significantly convoluted with residual current from oxygen reduction. Therefore, further analysis was limited to the first reduction peak. The return sweep reveals an oxidation peak corresponding to amine oxidation back to a nitro group. These results demonstrate the ability to electrochemically evaluate nitro-containing aromatic molecules in aqueous solutions.

Figure 4. Electroreduction of a single nitroaromatic group on TNT.

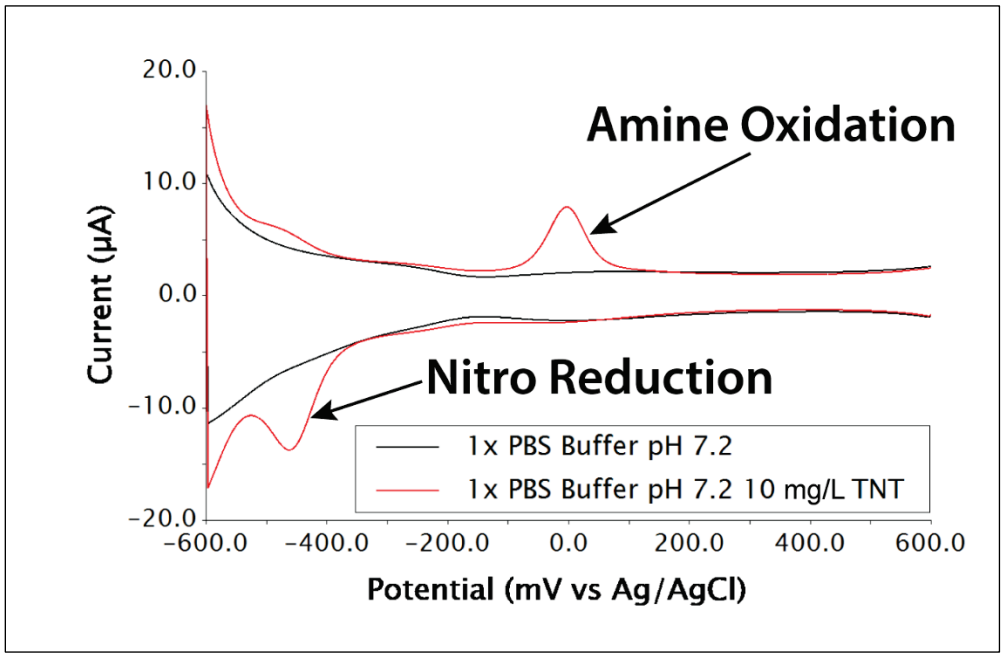

Since the overall nitroaromatic reduction reaction requires six proton transfer steps, it is highly dependent on the relative concentration of proton in the solution. To explore this effect and select an ideal buffer, the reaction was examined in acetate buffer (pH 5.85), carbonate buffer (pH 9.2), 1x PBS (pH 7.2), and KCl (pH 7.03) (Figure 5). A clear trend emerges in the buffered systems; the buffer with the greatest proton concentration (acetate) shows a peak at a lower thermodynamic potential (*ca.* -0.4 V vs Ag/AgCl), while the buffer with the lowest proton concentration (carbonate) shows a peak at a higher thermodynamic potential (*ca.* -0.5V vs Ag/AgCl). The trend is reversed for the oxidation process due to the reaction now producing protons, which is thermodynamically more favorable in more alkaline media according to Le Chatelier's principle. The reaction in unbuffered KCl with a measured pH of 7.03 reveals peaks at the most negative voltages. This could be explained by the lack of pH control directly adjacent to the electrode surface while the reaction is

occurring. Because residual oxygen reduction (which consumes protons) is occurring simultaneously with the nitroaromatic reduction (which also consumes protons), the pH directly adjacent to the electrode surface will vary significantly from the bulk pH. These data suggest the pH is drastically raised at the electrode surface in unbuffered solution, explaining the relative peak positions.

Figure 5. Effect of pH on the electroreduction of TNT.

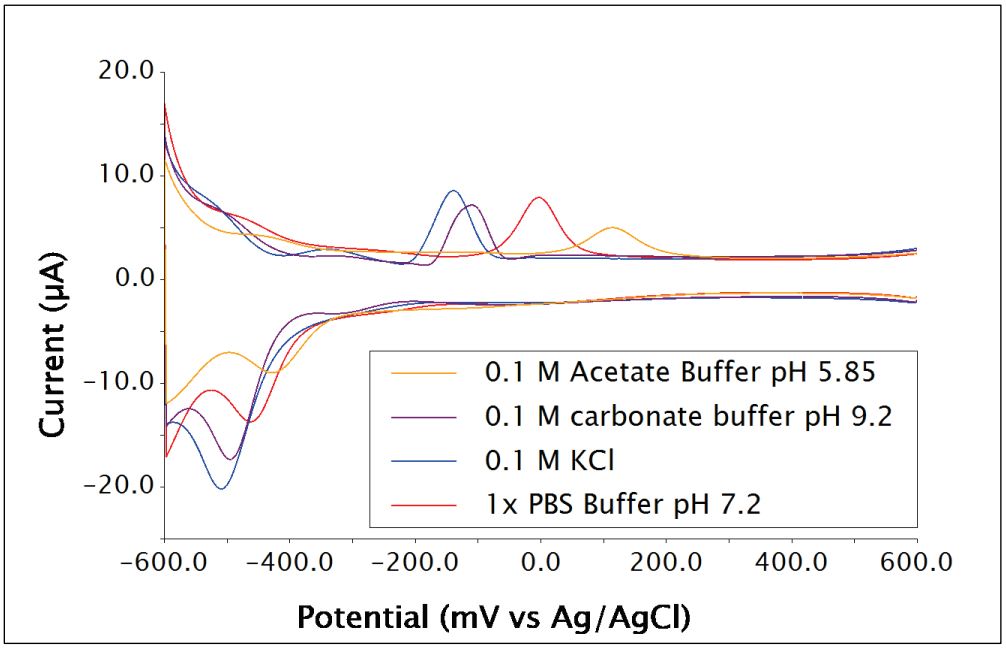

From these data, 1x PBS was chosen as an ideal buffer due to the enhanced peak height and more narrow peak width compared to acetate buffer, and more symmetric peak shape for the amine oxidation compared to carbonate buffer.

3.3 Electropolymerization and characterization of polyaniline-modified sensors

Electropolymerization of thin films may provide several significant advantages for chemical sensing. First, the molecular content of the polymer may enhance specific interactions between the electrode surface and the analyte of interest. For instance, acid-base interactions help drive association of acidic molecules such as 2,4-dichlorophenoxyacetic acid with poly(o-phenylenediamine) thin films (Fernando et al. 2021). Such interactions may serve to lower the overpotential to drive a specific electrochemical conversion, or permit a preconcentration effect to manifest as the analyte binds to the polymer. Second, if the polymer is

conductive, the surface area of the electrode may be greatly enhanced, enhancing the signal derived from analyte diffusion to the electrode surface. After characterizing the electrodes and buffers necessary to evaluate nitroaromatic compounds, a conductive aniline polymer film was electrodeposited to explore these potential benefits.

Figure 6a shows a voltammogram sweeping from -0.1 to 1.0 V vs Ag/AgCl for ten cycles to drive the growth of the polyaniline (PANI) film. The reaction was carried out in 0.5 M H_2SO_4 with 110 mM aniline monomer according to literature procedure (Wang et al. 2013) to drive the growth of a high-surface area thin film. Multiple characteristic peaks may be evaluated as the film grows. Since the polymerization initiates through the formation of a radical aniline cation at high potential, the electrochemical signal observed does not necessarily reflect the deposition of the film as non-conductive monomers (*e.g.*, *o*-phenylenediamine), but rather the electrochromic switching behavior (*i.e.*, the intrinsic electrochemistry) of the PANI precipitating onto the electrode surface. Once deposited, the conductive polymer may exist in a variety of oxidation states depending on the applied potential. The set of redox peaks between 0 and 0.2 V vs Ag/AgCl are associated with the conversion of the fully reduced leucoemeraldine base to the partially oxidized emeraldine, while the second set of redox peaks between 0.3 and 0.8 V vs. Ag/AgCl are related to the conversion of emeraldine to the fully oxidized pernigraniline base (Wang et al. 2013). The cycle number was restricted to ten cycles because thick polymer films formed by electrodeposition are prone to delamination. The film thickness will be optimized in future studies (See Chapter 4).

Figure 6. (a) Electropolymerization of aniline to form a conductive PANI film; (b) Micrograph of unmodified working electrode; (c) Post-PANI modification micrograph.

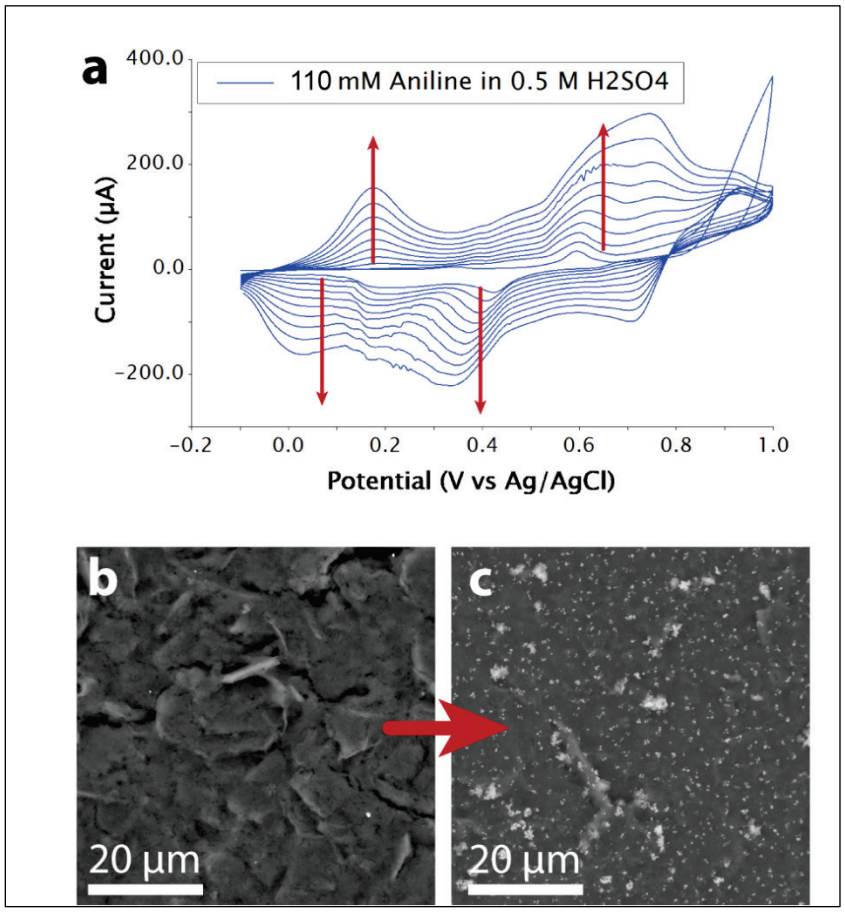

The resulting polymer film was evaluated using SEM by comparing an unmodified surface (Figure 6b) with a PANI modified surface (Figure 6c). The PANI-modified surface appears smoother than the unmodified graphitic surface and is characterized by polymer crystallites of various sizes, which appear to be approximately ~100 nm in agreement with previous literature (Wang et al. 2013). The combination of the characteristic electrochemical response for PANI films and change of surface structure *via* SEM confirm the successful deposition of a polymer layer.

It was hypothesized the electrochemical response of a conductive PANI film would exhibit a time-dependence due to reduced mass transfer of the analyte into the film, as well as potential adsorption/preconcentration effects due to intermolecular interactions (acid-base, π- π stacking, etc.) and hydrophilicity and hydrophobicity effects (*vide infra*). To test this hypothesis, the electrochemical reduction of DNAN was evaluated at a high concentration (10 mg/L) on the PANI-modified sensor in 1x PBS

(Figure 7). Two reduction peaks were evident over the background, which were related to the reduction of each nitro-group on DNAN (*vide infra*). Using a fresh electrode, the effect of preconcentration was examined by placing the electrode in the solution containing DNAN, waiting a specified period, and then running the electrochemical measurement. These data indicate it takes at least 5 min for the DNAN to fully permeate the PANI film based on the limiting peak current value, after which the current response does not increase appreciably. This effect is expected to show dependence on polymer properties such as film thickness, charge/oxidation state, and dopants. Therefore, it is essential to evaluate this to ensure sensors are compared at equilibrium.

Figure 7. Current magnitude as a function of incubation time demonstrating the preconcentration effect of DNAN within the PANI film.

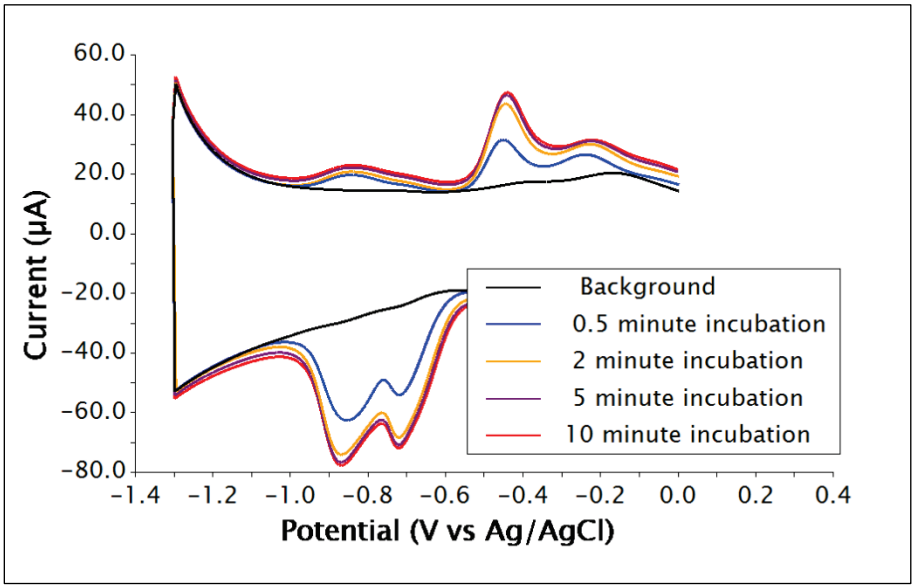

To remove the DNAN from the PANI film, the relative solubility of the reduced (amine-containing) compound versus the oxidized (nitro-containing) compound may be exploited. Figure 8 shows a voltammogram where a sensor saturated with DNAN was placed in a fresh buffer and swept over the same potential range used for detection. Due to the hydrophobicity of the nitro-containing molecule, it is likely that the preconcentration effect is driven in-part by the partitioning of DNAN into the PANI film. However, when DNAN is reduced to the amine-containing molecule, the hydrophobicity decreases (Pati et al. 2005), driving the species out of the polymer and regenerating a fresh interface. The result of this reduction process can be seen by the decreasing current signal, which approaches baseline values after only three sweeps. This cleaning

procedure was found to be highly reproducible for obtaining equivalent backgrounds using the PANI-modified electrode.

Figure 8. Electrochemical cleaning procedure to extract DNAN from the PANI-thin film.

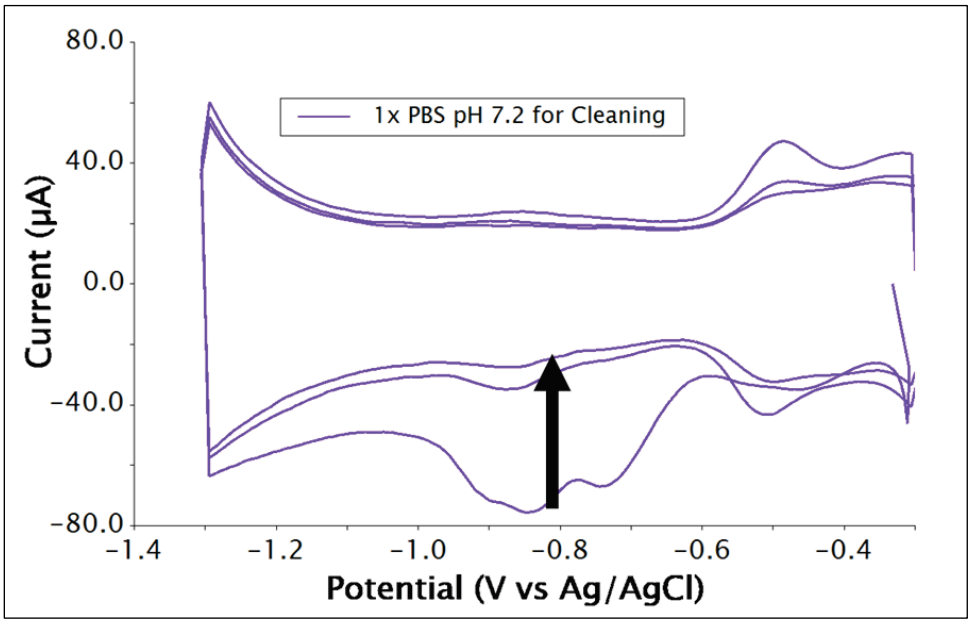

3.4 Detection of DNAN using polyaniline-modified sensors

With the electrochemical response of DNAN established on the PANI-modified sensor, trials with an unmodified sensor (i.e., a bare graphitic carbon surface) were undertaken to compare the relative analytical response. Figure 9 shows a comparison of two voltammograms with their respective backgrounds, one of 10 mg/L DNAN reduction on a bare graphitic carbon electrode, and the other on the PANI-modified sensor. A significant difference in baseline current was observed, which is related to the difference in capacitance between the high-surface area PANI film and the roughly planar graphitic carbon surface. Unfortunately, the slow relaxation kinetics of the polymer film resulted in this residual capacitance consistently observed across the PANI sensors; however, extending the pulse period longer than 50 ms to further subtract the capacitive signal causes a loss of Faradaic signal as the DNAN diffusion layer extends out and away from the electrode surface. Regardless, if a baseline measurement may be taken, the relative peak heights may be compared. The baseline-to-peak signal for the PANI-modified sensor is 4x that of the bare graphitic carbon electrode due to the surface area enhancement and preconcentration effects previously discussed.

Figure 9. Comparison of unmodified carbon electrode and the PANI-modified electrode revealing a 4x current enhancement.

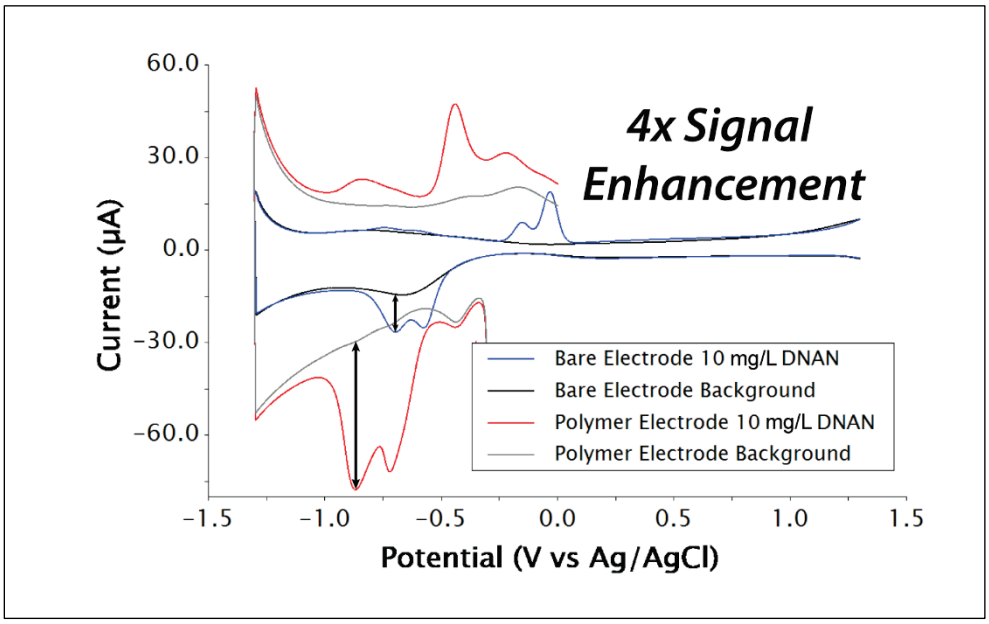

There may also be a kinetic component at play; note the convolution of the oxygen reduction signal in the background of the bare graphitic carbon trace with the 10 mg/L DNAN signal. Generally, Faradaic signals are additive when observed in voltammetry (i.e., the current from electron transfer process #1 is additive with electron transfer process #2); however, when reactive intermediates are produced (such as hydrogen peroxide in the case of oxygen reduction), it is possible that a post-electron transfer chemical reaction occurs which may depress the signal related to the analyte of interest (Zhou et al. 2018). Thus, the DNAN signal may be negatively influenced by the background oxygen reduction process. In contrast, the PANI-modified electrode shows a kinetic resistance to oxygen reduction at the potentials necessary to drive DNAN reduction, as evidenced by the lack of significant background peaks. This effect has been documented previously using a Tafel analysis, which indicates O_2 reduction to H_2O_2 is favored on bare graphitic carbon electrodes compared to PANI-modified electrodes (Cui and Lee 1994). While unfortunate for catalytic applications, this suppression of the oxygen reduction reaction is favorable for deconvoluted chemical sensing.

The advantages of the PANI-modified electrode were employed to detect trace levels of DNAN in 1x PBS buffer. A slight increase in current is visible for the iterative addition of 100, 200, and 300 µg/L µg/L DNAN with a 5-min preconcentration timeframe (Figure 10). However, the increase in

current is convoluted by the slight change in capacitive signal and the slope of the baseline. Applying a background correction in this case may cause a convolution of the capacitive and Faradaic signals, which could mask trends in the signal related to DNAN reduction.

Figure 10. Reduction of DNAN at a PANI-modified surface after a 5-min preconcentration timeframe.

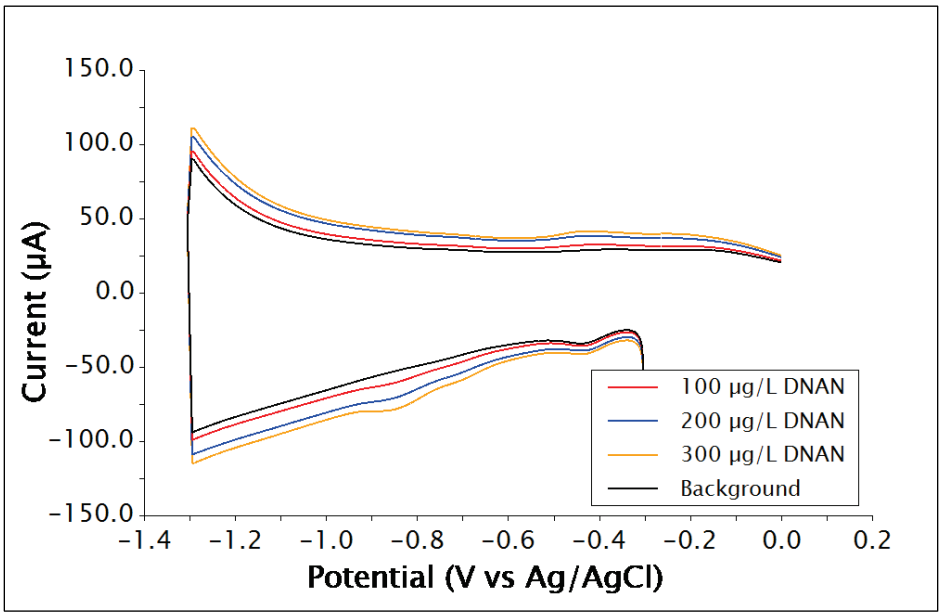

Provided a reference peak is available to level-shift the data, the capacitance may be corrected. Though adding an internal standard like ferrocene methanol is an option, the appearance of a surface peak at *ca.* -0.4 V vs Ag/AgCl that was consistent in the background and calibration points was noted. This background peak was likely associated with a surface process in the electroactive polymer, as it does not appear in the background voltammograms on bare carbon surfaces. Thus, the peak of this surface wave was used as a zero-point for the data prior to background correction (Figure 11a). The background has been subtracted and does not appear on this plot (Figure 11a) as all values are normalized to a y-value of 0. Here, the dual wave reduction of DNAN is much more apparent and increases linearly with the concentration of DNAN. The calibration curve developed from these data shows linearity with an R^2 of 0.9991 and a slope of 62.7 nA/µg/L (Figure 11b). The limit of detection (LOD) was calculated using the following formula:

$$LOD = \frac{3 * \sigma_{signal}}{b}$$

Where σ_{signal} is the standard deviation of the electrochemical signal (i.e., the noise), and b is the slope of the calibration curve (Sanagi et al. 2019). This formula suggests a LOD on the order of ~2 µg/L with an LOQ (10x the noise divided by the slope) of 5 µg/L. This value represents a remarkable detection capability for an electrochemical sensor using direct reductive detection and reflects the power of using a polymer film as a preconcentration medium. Since the thickness of the polymer film will affect the detection efficiency, the calibration experiments were run once to demonstrate a proof-of-concept for the enhanced sensitivity offered by the PANI-modified sensor. Future work will focus on optimizing the thickness and stability of the PANI film and evaluating the sensors in triplicate to determine the extent of sensor-to-sensor heterogeneity. Because the surface area will be difficult to control in a three-dimensional polymer network, additional characterization techniques such as electrochemical impedance spectroscopy (EIS) may be necessary to normalize the current by area to improve reproducibility (Musiani 1990).

Figure 11. (a) Baseline corrected and subtracted SWVs from Figure 10; (b) Calibration curve obtained from the SWV data.

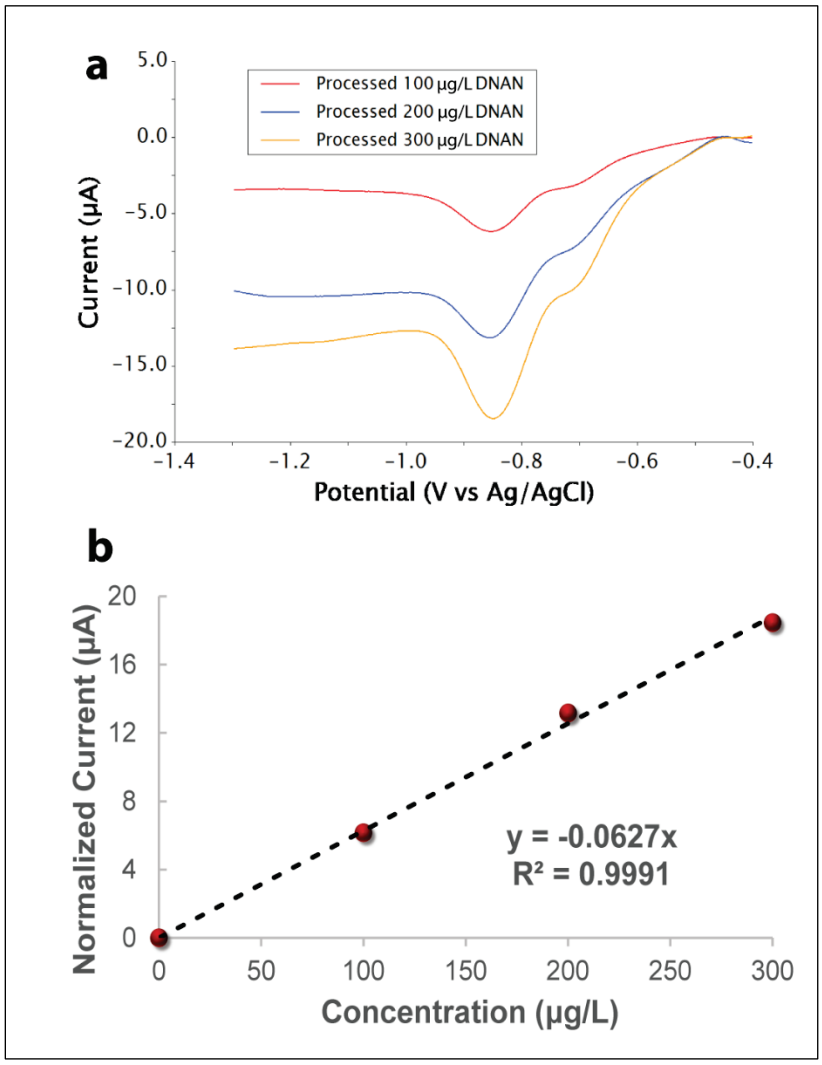

3.5 Assessment of DNAN/polyaniline molecularly imprinted polymer (MIP) sensor

Molecularly imprinted polymers (MIPs) are formed by polymerizing a monomer in the presence of a template molecule generating specific recognition interactions (e.g., acid-base, hydrogen bonding) within the polymer film (Malitesta et al. 2012). The authors hypothesized that polymerizing aniline in the presence of DNAN would enhance the surface area of the polymer film due to dopant effects. Furthermore, after stripping the DNAN away, we believed the binding properties for DNAN would be enhanced by the so-called "pockets" in the imprinted polymer film with a specific affinity for DNAN (Fernando et al. 2021; Glasscott et al. 2020). The exact mechanism for heightened re-adsorption affinity into

molecularly imprinted polymers is still an open question (Sharma et al. 2019). Thus, the combination of a higher surface area with increased binding affinity should, in theory, enhance the preconcentration effect and enable more sensitive measurements.

The synthesis of the MIP-modified graphitic carbon sensor was carried out under equivalent conditions as the non-imprinted polyaniline film, hereafter referred to as the non-imprinted polymer (NIP). Figure 12 shows the electrochemical growth of the MIP film over 10 cycles. Immediately evident is the difference in inherent redox activity for the MIP compared to the NIP. While the first oxidation step to form the emeraldine base appears similar, the following oxidation of emeraldine to the fully oxidized pernigraniline base appears more kinetically facile. Notably, no waves observed correspond to the oxidation of DNAN based on the growth of each peak over time and gaussian peak shape traditionally associated with surface processes (such as PANI conversion to various oxidation states). Because the second oxidation process is a convolution of multiple peaks, it is difficult to determine the exact mechanism. However, the alteration of the electropolymerization response after introduction of the DNAN dopant is consistent with previous studies and indicates the successful formation of an imprinted electrode (Liao et al. 2019).

Figure 12. Overlay of electropolymerization voltammograms for the MIP and NIP.

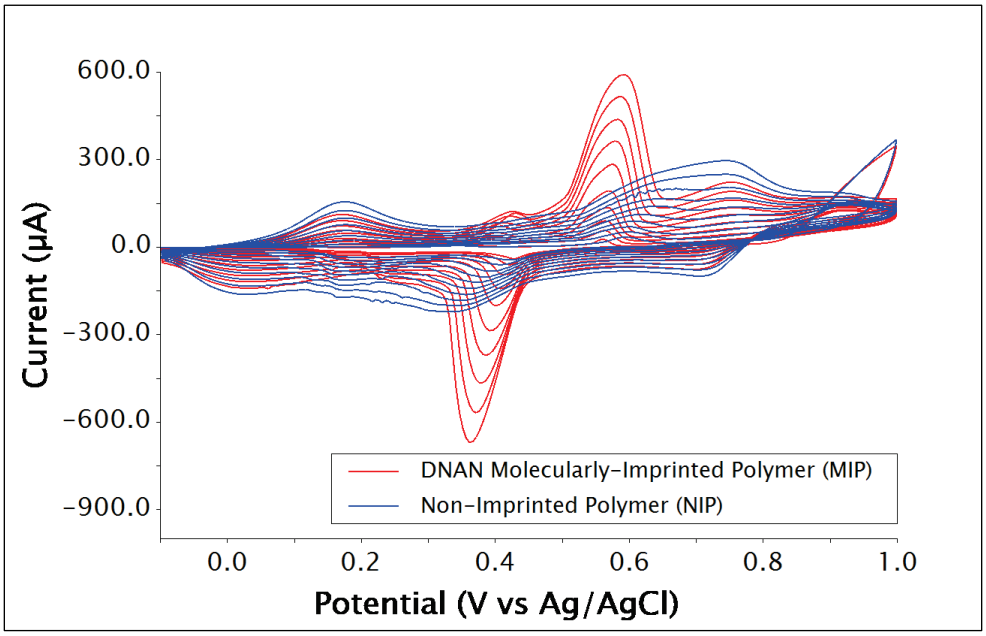

After functionalizing the sensor with the DNAN/PANI MIP and extracting via the cleaning method described above in fresh buffer, the background wave shown in Figure 13 was obtained at a relatively high background current (80 µA) compared to the background current for the NIP (30 µA), suggesting a higher relative surface area. The increase in surface area compared to the NIP agrees with previous studies introducing dopants into PANI films (Shi et al. 2015). DNAN was then introduced into the solution at a concentration of 0.25 mg/L to probe the electrochemical response. After a 5-min incubation period, the background current decreased precipitously. Further addition to a total concentration of 0.5 mg/L DNAN caused another drop in background current, which brought it back to the ~30 µA baseline observed for the NIP. Interestingly, further addition to 1 ppm and 3.5 mg/L caused slight increases in the peak height, reversing the previous trend.

Figure 13. Competing current/capacitive responses for the MIP at various concentrations of DNAN.

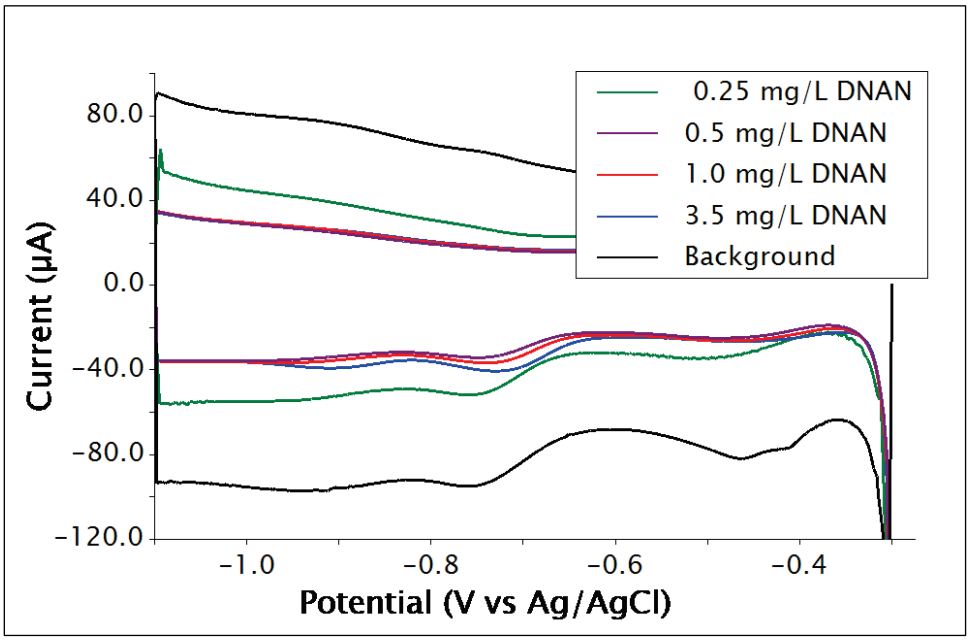

The change in peak height is plotted in Figure 14, which suggests a transition from a capacitively dominated process to an electron-transfer dominated process. Mechanistically, it is possible the low concentration of DNAN re-adsorbing into the DNAN/PANI MIP film prompts a structural/morphological change reducing the capacitance. Eventually, this effect competes with the Faradaic reduction process, causing the peak current to rebound slightly. Since SWV is a background-subtraction technique, assessing capacitive behavior is not ideal, and other techniques

such as EIS and DC voltammetry will be used in future work. While the desired response was not immediately obtained, the MIP film results showed promise for developing more sensitive and potentially selective sensors based on the reduction of a capacitive signal. Future work will focus on understanding the process driving the reduction in capacitance via correlated electrochemical, ellipsometric, and quartz crystal microbalance methods.

Figure 14. Peak current versus concentration of DNAN revealing capacitive/electron transfer competition.

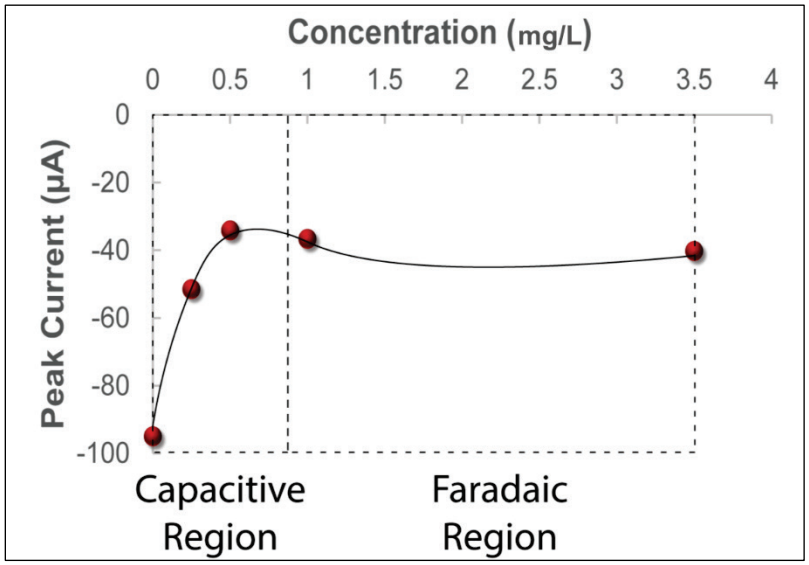

3.6 Evaluation of PETN in liquid-liquid extraction amenable 1,2-dichloroethane

While direct reduction of DNAN in aqueous systems represents a straightforward detection method, explosive compounds, which are practically insoluble in water, such as pentaerythritol tetranitrate (PETN), represent a more difficult analyte for electrochemical detection. Furthermore, the structure of PETN contains nitrate ester groups as opposed to nitroaromatic groups, meaning electrochemical reduction will require a higher potential magnitude (Galik et al. 2011). Control experiments for PETN in aqueous systems showed no change in electrochemical signal over the background. Thus, electrochemistry in an organic solvent was pursued to increase the concentration of PETN to detectable levels, and to increase the accessible potential window for electroreduction of the PETN. 1,2-dichloroethane was chosen due to its immiscibility with water, which may permit the development of liquid-liquid extraction-based sensors in the future (Sabaragamuwe et al. 2020).

In this experiment, a large aqueous sample could be mixed with a smaller volume of 1,2-dichloroethane to partition trace concentrations from the aqueous phase to the organic phase for electrochemical detection.

To evaluate the electroreduction of PETN in 1,2-dichloroethane, the electrochemical window for 1,2-dichloroethane versus a silver/silver ion electrode was examined. This silver/silver ion reference electrode is commonly employed in non-aqueous solvents due to the instability of Ag/AgCl reference electrodes in these matrices (Elgrishi et al. 2018). The background showed characteristics of oxygen reduction (likely to superoxide radical [Galiote et al. 2014]), and reduction of either the salt (tetrabutylammonium cation) or the 1,2-dichloroethane itself at *ca.* 1.4 V vs Ag/Ag^+. The solution was purged with argon to clearly evaluate the reduction of PETN to reduce the interference of the oxygen reduction signal. Figure 15a shows a series of voltammograms over different concentrations of PETN, which give a linear increase in peak height at *ca.* 1.25 V versus Ag/Ag^+. These peaks do not show reversibility as one might expect for the one electron reduction of a nitro group in aprotic solvent to form a nitro radical (Olson et al. 2015). Since there is no proton source, the traditional reduction of a nitro group to an amine is likely not occurring appreciably. Furthermore, since there is no aromatic ring to help stabilize the radical, it is likely a kinetically rapid inter- or intra-molecular reaction takes place by which the radical is consumed (Wirtanen et al. 2020). While the exact mechanism of reduction and reaction product is unclear, a calibration curve may be generated with an R^2 of 0.9978, where the non-zero y-intercept represents the capacitive current in the background (Figure 15b). All experiments were run in triplicate, and the standard deviation of the blank (35 nA) showed agreement with the noise profile (35 nA), indicating excellent repeatability. Using these values, a LOD of 500 µg/L was obtained.

Figure 15. (a) Cyclic voltammograms at various concentrations of PETN in deaerated 1,2-dichloroethane; (b) Calibration curve tracking the peak height as a function of concentration.

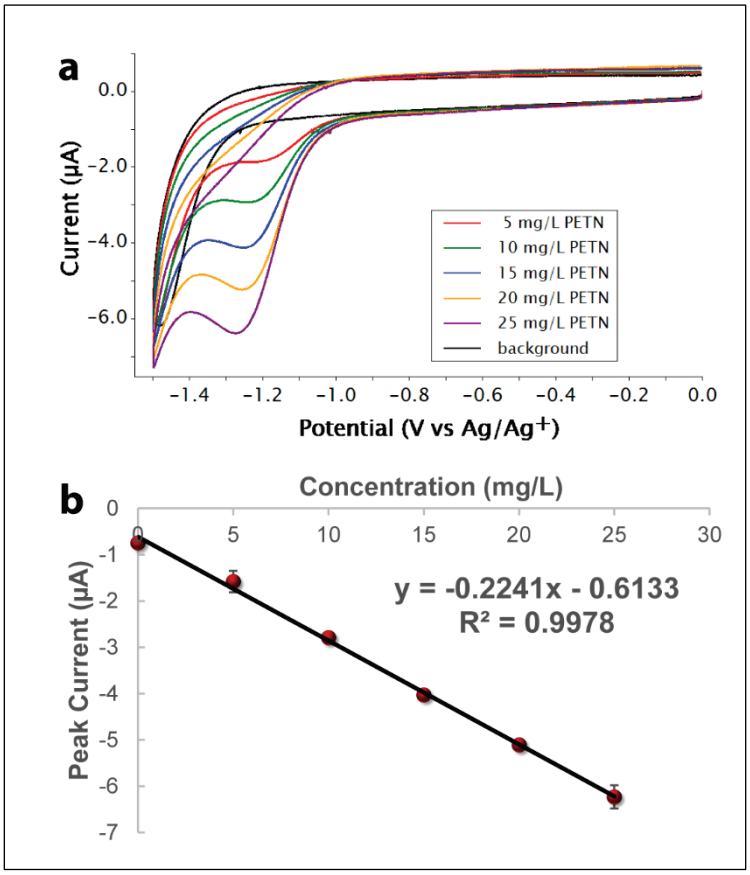

To further probe the nature of the reaction, a scan rate analysis was performed to elucidate whether an adsorption process was occurring at the electrode surface versus a diffusion process related to the PETN reduction. Cyclic voltammetry's (CVs) were performed for a PETN concentration of 25 mg/L at six scan rates ranging from 10 mV/s to 500 mV/s (Figure 16). As expected, the peak height grows at higher scan rates due to the decreased time interval over which the PETN at the electrode surface is reduced. Since the current is inversely proportional to time ($I = C\,t^{-1}$, where I is the current, C is the charge in coulombs, and t is the time), faster scan rates produce higher current responses. This dependence will trend linearly with either the scan rate directly or the square-root of the scan rate. If the process is surface/adsorption controlled (i.e., oxidation of leucoemeraldine base to emeraldine base in a PANI film), the peak current will trend with the scan rate directly due to the confined nature of the analyte. However, if the arrival of the analyte at the electrode surface is diffusion controlled, the Einstein equation predicts a dependance on the

square-root of time. Thus, diffusion-controlled processes will see a peak current increase linearly with the square-root of the scan rate.

Figure 16. Scan rate analysis to determine diffusion versus surface control.

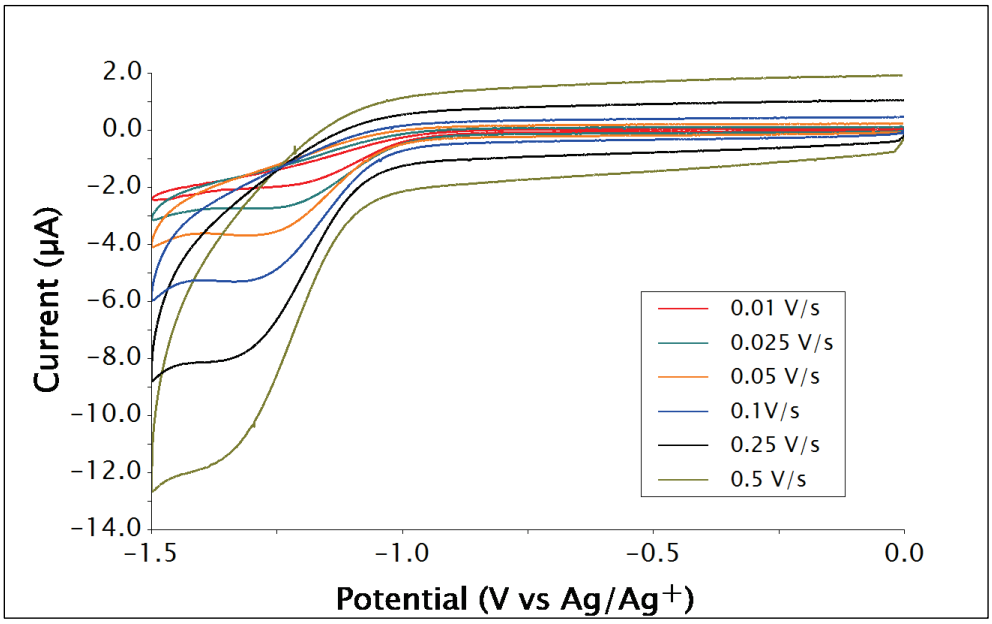

Figures 17a and b show the peak current plotted versus the scan rate and square-root of the scan rate, respectively, revealing a greater linear dependence on the square-root of the scan rate. These data suggest the PETN arrives at the surface via diffusion and undergoes an electron transfer process (likely 1 electron to form a radical).

Figure 17. (a) Non-linear trend for peak current plotted against the scan; (b) Linear trend for peak current for PETN reduction plotted against the square-root of the scan rate.

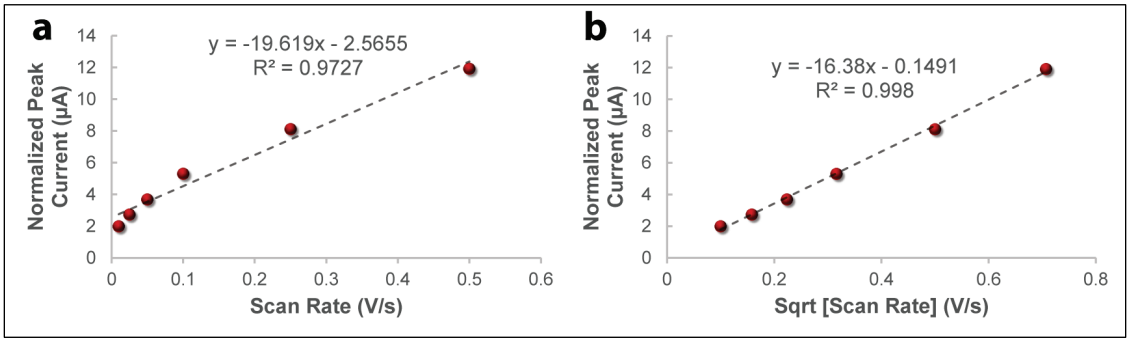

As a control experiment, the capacitive signal (which is a surface process) was also tracked and revealed a typical anodic and cathodic trend scaling directly with the scan rate (Figure 18). Since the PETN reduction process is diffusion-controlled, the Randles-Sevcik equation (*vide supra*) may be

used to estimate the diffusion coefficient, which renders a value of 6.57 x 10^{-6} cm/s. Though no values for the diffusion coefficient of PETN exist in the literature for 1,2-dichloroethane, this value is remarkably close to the diffusion coefficient of pentaerythritol mononitrate of 6.67 x 10^{-6} cm/s reported for aqueous systems (Jarrell and Carignan 1966).

Figure 18. Control experiment assessing the anodic and cathodic capacitive current signal (surface controlled) as a function of scan rate.

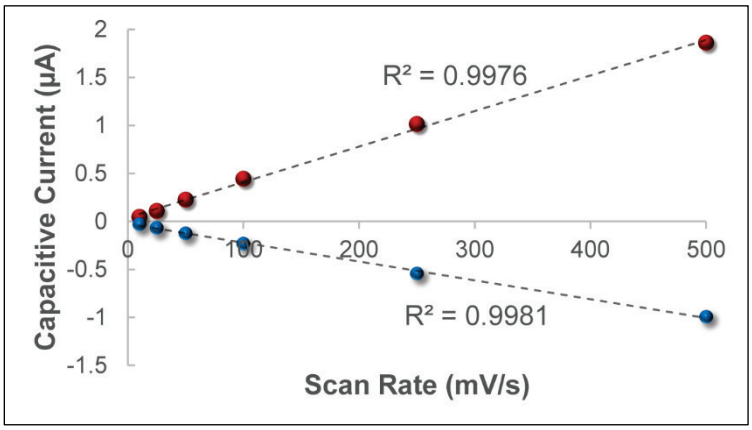

4 Conclusions and Future work

In this work, two proof-of-concept electroanalytical methods for the quantification of 2,4-dinitroanisol (DNAN) and pentaerythritol tetranitrate (PETN) were demonstrated. For the first time, DNAN reduction was analyzed and compared at a bare graphitic carbon electrode, a polyaniline-modified electrode, and a molecularly imprinted polymer electrode. We hypothesized the electrochemical signal related to the reduction of nitroaromatic groups would be enhanced at a PANI-modified electrode due to enhanced surface area, as well as interactions between the DNAN and PANI driving a preconcentration effect. Both mechanisms were confirmed to manifest a 4x greater analytical signal compared to the bare electrode. Additionally, this preconcentration effect permitted the detection of DNAN down to 100 µg/L, with a detection limit of 2 µg/L. However, while it was thought imprinting the PANI film with DNAN molecules would further enhance these effects, a convolution characterized by competition between the decreasing capacitive signal and the increasing electron transfer signal was observed.

Future work will address the three priorities listed below for the detection of DNAN at polymer-modified electrodes.

1. The polymer thickness and morphology must be optimized and correlated to the equilibration timeframe and current signal to obtain a sensor with a minimal incubation period and a maximal LOD.
2. The surface area of the PANI films must be quantified to improve sensor-to-sensor response.
3. The capacitive signal and electron transfer signal for the MIP-modified electrode must be deconvoluted using electrochemical impedance spectroscopy or other advanced electrochemical techniques to determine if an ultra-sensitive method can be extracted from these unique surfaces.

The electrochemical response of PETN was evaluated in deaerated 1,2-dichloroethane to overcome solubility issues in aqueous systems, as well as electrochemical potential window limits. A calibration curve was generated between 5 and 25 mg/L with an LOD of 500 µg/L, and a scan rate analysis revealed a diffusion-controlled process. Using the Randles Sevcik equation, a diffusion coefficient of 6.57×10^{-6} cm/s was extracted,

which agreed with previous values for the similarly structured pentaerythritol mononitrate.

Future work will address the two priorities listed below for PETN detection.

1. A liquid-liquid extraction experiment should be attempted to quantify the partition coefficient of PETN into 1,2-dichloroethane to demonstrate the viability of an extraction-based sensing method.
2. The product of the reduction process should be isolated and evaluated via mass spectrometry to clearly determine the electron transfer mechanism.

References

Bard, A. J., and L. R. Faulkner. 2001. *Electrochemical Methods: Fundamentals and Applications*. 2 ed.. New York, NY: John Wiley & Sons.

Cannes, C ., F. Kanoufi, and A. J. Bard. 2003. "Cyclic voltammetry and scanning electrochemical microscopy of ferrocenemethanol at monolayer and bilayer-modified gold electrodes." *Journal of Electroanalytical Chemistry*, 547 (1): 83-91.

Cui, C. Q., and J. Y. Lee. 1994. "Effect of polyaniline on oxygen reduction in buffered neutral solution." *Journal of Electroanalytical Chemistry*, 367 (1): 205-212.

Dasary, S. S. R ., A. K. Singh, D. Senapati, H. Yu, and P. C. Ray. 2009. "Gold nanoparticle based label-free sers probe for ultrasensitive and selective detection of trinitrotoluene." *Journal of the American Chemical Society*, 131 (38): 13806-13812.

de Levie, R. 1963. "On porous electrodes in electrolyte solutions: I. capacitance effects." *Electrochimica Acta*, 8 (10): 751-780.

Demeritte, T ., R. Kanchanapally, Z. Fan, A. K. Singh, D. Senapati, M. Dubey. E. Zakar, and P. C. Ray. 2012. "Highly efficient sers substrate for direct detection of explosive TNT using popcorn-shaped gold nanoparticle-functionalized swcnt hybrid." *Analyst*, 137 (21): 5041-5045.

Eiceman, G. A ., E. V. Krylov, N. S. Krylova, E. G. Nazarov, and R. A. Miller. 2004. "Separation of ions from explosives in differential mobility spectrometry by vapor-modified drift gas." *Analytical Chemistry*, 76 (17): 4937-4944.

Elgrishi, N ., K. J. Rountree, B. D. McCarthy, E. S. Rountree, T. T. Eisenhart, and J. L. Dempsey. 2018. "A practical beginner's guide to cyclic voltammetry." *Journal of Chemical Education*, 95 (2): 197-206.

Ewing, R. G ., B. H. Clowers, and D. A. Atkinson. 2013. "Direct real-time detection of vapors from explosive compounds." *Analytical Chemistry*, 85 (22): 10977-10983.

Fernando, P. U. A. I ., E. Alberts, M. W. Glasscott, A. Netchaev, J. D. Ray, K. Conley, R. Patel, J. Fury, D. Henderson, L. C. Moores, and G. Kosgei. 2021. "In Situ Preconcentration and Quantification of Cu2+ Via Chelating Polymer-Wrapped Multiwalled Carbon Nanotubes." *ACS Omega*, 6 (8): 5158-5165.

Fernando, P. U. A. I ., M. W. Glasscott, G. K. Kosgei, J. S. Cobb, E. M. Alberts, C. G. Bresnahan, T. C. Schutt, G. W. George, and L. C. Moores. 2021. "Toward rational design of electrogenerated molecularly imprinted polymers (emips): Maximizing monomer/template affinity." *ACS Applied Polymer Materials*.

Fernando, P. U. A. I ., M. W. Glasscott, K. Pokrzywinski, B. M. Fernando, G. K. Kosgei, and L. C. Moores. 2021. "Analytical methods incorporating molecularly imprinted polymers (Mips) for the quantification of microcystins: A mini-review." *Critical Reviews in Analytical Chemistry*, 1-15.

Forzani, E. S ., D. Lu, M. J. Leright, A. D. Aguilar, F. Tsow, R. A. Iglesias, Q. Zhang, J. Lu, J. Li, and N. Tao. 2009. "A hybrid electrochemical–colorimetric sensing platform for detection of explosives." *Journal of the American Chemical Society*, 131 (4): 1390-1391.

Galik, M ., A. M. O'Mahony, and J. Wang. 2011. "Cyclic and square-wave voltammetric signatures of nitro-containing explosives." *Electroanalysis*, 23 (5): 1193-1204.

Galiote, N. A ., D. C. de Azevedo, O. N. Oliveira, and F. Huguenin. 2014. "Investigating the kinetic mechanisms of the oxygen reduction reaction in a nonaqueous solvent." *The Journal of Physical Chemistry C*, 118 (38): 21995-22002.

Glasscott, M. W ., A. D. Pendergast, and J. E. Dick. 2018. "A universal platform for the electrodeposition of ligand-free metal nanoparticles from a water-in-oil emulsion system." *ACS Applied Nano Materials*, 1 (10): 5702-5711.

Glasscott, M. W ., K. J. Vannoy, P. U. A. Iresh Fernando, G. K. Kosgei, L. C. Moores, and J. E. Dick. 2020. "Electrochemical sensors for the detection of fentanyl and its analogs: Foundations and recent advances." *TrAC Trends in Analytical Chemistry*, 116037.

Glasscott, M. W ., K. J. Vannoy, R. Kazemi, M. D. Verber, and J. E. Dick. 2020. "M-Mip: Molecularly imprinted polymer-modified microelectrodes for the ultrasensitive quantification of genx (Hfpo-Da) in river water." *Environmental Science & Technology Letters*, 7 (7): 489-495.

Glasscott, M. W ., M. D. Verber, J. R. Hall, A. D. Pendergast, C. J. McKinney, and J. E. Dick. 2020. :Sweepstat: A build-it-yourself, two-electrode potentiostat for macroelectrode and ultramicroelectrode studies." *Journal of Chemical Education*, 97 (1): 265-270.

Glasscott, M. W., and J. E. Dick. 2021. "Electrodeposition in aqueous nanoreactors." *Current Opinion in Electrochemistry*, 25, 100637.

Hawari, J ., F. Monteil-Rivera, N. N. Perreault, A. Halasz, L. Paquet, Z. Radovic-Hrapovic, S. Deschamps, S. Thiboutot, and G. Ampleman. 2015. "Environmental fate of 2,4-dinitroanisole (Dnan) and its reduced products." *Chemosphere*, 119: 16-23.

Jarrell, J. R., and Y. P. Carignan. 1966. *Polarographic Study of Nitrate Esters. I. Reduction of Pentaerythritol Mononitrate*; PICATINNY ARSENAL DOVER NJ PROPELLANTSLAB.

Liao, G ., Q. Li, and Z. Xu. 2019. "The chemical modification of polyaniline with enhanced properties: A review." *Progress in Organic Coatings*, 126, 35-43.

Malitesta, C ., E. Mazzotta, R. A. Picca, A. Poma, I. Chianella, and S. A. Piletsky. 2012. "Mip sensors – the electrochemical approach." *Analytical and Bioanalytical Chemistry*, 402 (5): 1827-1846.

Musiani, M. M. 1990. "Characterization of electroactive polymer layers by electrochemical impedance spectroscopy (Eis)." *Electrochimica Acta*, 35 (10): 1665-1670.

Ngamchuea, K ., S. Eloul, K. Tschulik, and R. G. Compton. 2014. "Planar diffusion to macro disc electrodes—What electrode size is required for the Cottrell and Randles-Sevcik Equations to apply quantitatively?" *Journal of Solid State Electrochemistry*, 18 (12): 3251-3257.

Olivares, C ., J. Liang, L. Abrell, R. Sierra-Alvarez, and J. A. Field. 2013. "Pathways of reductive 2,4-dinitroanisole (Dnan) biotransformation in sludge." *Biotechnology and Bioengineering*, 110 (6): 1595-1604.

Olson, E. J ., W. C. Isley, J. E. Brennan, C. J. Cramer, and P. Bühlmann. 2015. "Electrochemical reduction of 2,4-dinitrotoluene in aprotic and Ph-buffered media." *The Journal of Physical Chemistry C*, 119 (23): 13088-13097.

Pati, H. N ., H. L. Holt, R. LeBlanc, J. Dickson, M. Stewart, T. Brown, and M. Lee. 2005. "Synthesis and cytotoxic properties of nitro- and aminochalcones." *Medicinal Chemistry Research*, 14 (1): 19-25.

Perreault, N. N ., D. Manno, A. Halasz, S. Thiboutot, G. Ampleman, and J. Hawari. 2012. "Aerobic biotransformation of 2,4-dinitroanisole in soil and soil bacillus sp." *Biodegradation*, 23 (2): 287-295.

Sabaragamuwe, S. G ., H. Madawala, S. R. Puri, and J. Kim. 2020. "Towards ultralow detection limits of aromatic toxicants in water using pluronic nanoemulsions and single-entity electrochemistry." *Analytica Chimica Acta*, 1139, 129-137.

Sanagi, M. M ., S. L. Ling, Z. Nasir, D. Hermawan, W. A. Wan Ibrahim, and A. A. Naim. 2019. "Comparison of signal-to-noise, blank determination, and linear regression methods for the estimation of detection and quantification limits for volatile organic compounds by gas chromatography." *Journal of AOAC INTERNATIONAL*, 92 (6): 1833-1838.

Sharma, P. S ., A. Garcia-Cruz, M. Cieplak, K. R. Noworyta, and W. Kutner. 2019. "'Gate Effect' in molecularly imprinted polymers: The current state of understanding." *Current Opinion in Electrochemistry*, 16, 50-56.

Shi, L ., A. G. Hou, L. Y. Chen, and Z. F. Wang. 2015. "Electrochemical sensor prepared from molecularly imprinted polymer for recognition of TNT." *Polymer Composites*, 36 (7): 1280-1285.

Stanley, J. K., G. R. Lotufo, J. M. Biedenbach, P. Chappell, and K. A. Gust. 2015. "Toxicity of the conventional energetics TNT and Rdx relative to new insensitive munitions constituents DNAN and Nto in Rana Pipiens tadpoles." *Environmental Toxicology and Chemistry*, 34 (4): 873-879.

Tam, M., and H. H. Hill. 2004. "Secondary electrospray ionization-ion mobility spectrometry for explosive vapor detection." *Analytical Chemistry*, 76 (10): 2741-2747.

Wang, J ., B. Tian, V. B. Nascimento, and L. Angnes. 1998. "Performance of screen-printed carbon electrodes fabricated from different carbon inks." *Electrochimica Acta*, 43 (23): 3459-3465.

Wang, S ., S. Lu, X. Li, X. Zhang, S. He, and T. He. 2013. "Study of H2so4 concentration on properties of H2so4 doped polyaniline counter electrodes for dye-sensitized solar cells." *Journal of Power Sources*, 242: 438-446.

Wirtanen, T ., E. Rodrigo, and S. R. Waldvogel. 2020. "Recent advances in the electrochemical reduction of substrates involving N–O bonds." *Advanced Synthesis & Catalysis*, 362 (11): 2088-2101.

Zhou, Y ., X. Liu, W. Jiang, and Y. Shu. 2018. "Theoretical insight into reaction mechanisms of 2,4-dinitroanisole with hydroxyl radicals for advanced oxidation processes." *Journal of Molecular Modeling*, 24 (2): 44.

Zhuang, L ., L. Gui, and R. W. Gillham. 2008. "Degradation of pentaerythritol tetranitrate (Petn) by granular iron." *Environmental Science & Technology*, 42 (12): 4534-4539.

Acronyms and Abbreviations

Ag/AgCl	Ag/AgCl
Ag/Ag^+	Silver/Silver Ion
CSWV	Cyclic Square Wave Voltammetry
CV	Cyclic voltammetry
DNAN	2,4-Dinitroanisol
EL	Environmental Laboratory
ERDC	US Army Engineer Research and Development Center
IMS	Ion Mobility Spectroscopy
LOD	Limit of Detection
LOQ	Limit of Quantitation
MIP	Molecularly Imprinted Polymer
MS	Mass Spectrometry
NIP	Non-Imprinted Polymer
PANI	Polyaniline
PBS	Phosphate Buffered Saline
PETN	Pentaerythritol Tetranitrate
RDX	1,3,5-Trinitro-1,3,5-Triazine
SERS	Surface Enhanced Raman Spectroscopy
SEM	Scanning Electron Microscopy

SPE	Screen-Printed Electrode
SWV	Square Wave Voltammetry
TNT	2,4,6-trinitrotoluene

REPORT DOCUMENTATION PAGE

Form Approved
OMB No. 0704-0188

1. REPORT DATE (DD-MM-YYYY)
March 2022

2. REPORT TYPE
Final Report

3. DATES COVERED (From - To)

4. TITLE AND SUBTITLE
Toward the Electrochemical Detection of 2,4-Dinitroanisole (DNAN) and Pentaerythritol Tetranitrate (PETN)

5a. CONTRACT NUMBER

5b. GRANT NUMBER

5c. PROGRAM ELEMENT
U452567

6. AUTHOR(S)
Matthew W. Glasscott, Johanna N. Jernberg, Erik M. Alberts, and Lee C. Moores

5d. PROJECT NUMBER
494498

5e. TASK NUMBER
A1000

5f. WORK UNIT NUMBER

7. PERFORMING ORGANIZATION NAME(S) AND ADDRESS(ES)
US Army Engineer Research and Development Center (ERDC)
Environmental Laboratory (EL)
3909 Halls Ferry Rd, Vicksburg, MS 39180-6199

Oak Ridge Institute for Science and Education
1299 Bethel Valley Rd., Oak Ridge, TN 37830

SIMETRI
7005 University Blvd., Winter Park, FL 32792

8. PERFORMING ORGANIZATION REPORT NUMBER
ERDC/EL TR-22-3

9. SPONSORING / MONITORING AGENCY NAME(S) AND ADDRESS(ES)
Headquarters, U.S. Army Corps of Engineers
Washington, DC 20314-1000

10. SPONSOR/MONITOR'S ACRONYM(S)

11. SPONSOR/MONITOR'S REPORT NUMBER(S)

12. DISTRIBUTION / AVAILABILITY STATEMENT
Approved for public release; distribution is unlimited.

13. SUPPLEMENTARY NOTES

14. ABSTRACT

Analytical methods to rapidly detect explosive compounds with high precision are paramount for applications ranging from national security to environmental remediation. This report demonstrates two proof-of-concept electroanalytical methods for the quantification of 2,4-dinitroanisol (DNAN) and pentaerythritol tetranitrate (PETN). For the first time, DNAN reduction was analyzed and compared at a bare graphitic carbon electrode, a polyaniline-modified (PANI) electrode, and a molecularly imprinted polymer (MIP) electrode utilizing PANI to explore the effect of surface-area and preconcentration affinity on the analytical response.

Since some explosive compounds such as PETN are not appreciably soluble in water (<10 μg/L), necessitating a different solvent system to permit direct detection *via* electrochemical reduction. A 1,2-dichloroethane system was explored as a possibility by generating a liquid-liquid extraction-based sensor exploiting the immiscibility of 1,2-dichloroethane and water. The reduction process was explored using a scan rate analysis to extract a diffusion coefficient of 6.67×10^{-6} cm/s, in agreement with literature values for similarly structured nitrate esters.

Once further refined, these techniques may be extended to other explosives and combined with portable electrochemical hardware to bring real-time chemical information to soldiers and citizens alike.

15. SUBJECT TERMS
Explosives, Military – Environmental aspects
Explosives, Military – Residues – Detection
Electrochemical sensors
Electrolytic reduction

16. SECURITY CLASSIFICATION OF:			17. LIMITATION OF ABSTRACT	18. NUMBER OF PAGES	19a. NAME OF RESPONSIBLE PERSON
a. REPORT	b. ABSTRACT	c. THIS PAGE			19b. TELEPHONE NUMBER (include area code)
Unclassified	Unclassified	Unclassified	SAR	42	